3-D Characterization of Seismic Properties at the Smart Weapons Test Range, YPG

October 2001

Richard D. Miller,* Thomas S. Anderson,** John C. Davis,* Don W. Steeples,† Mark L. Moran**
*Kansas Geological Survey, †Department of Geology, University of Kansas, Lawrence, Kansas 66045
**U.S. Army Corps of Engineers, CRREL, 72 Lyme Road, Hanover, New Hampshire 03755

ABSTRACT

The Smart Weapons Test Range (SWTR) lies within the Yuma Proving Ground (YPG), Arizona. SWTR is a new facility constructed specifically for the development and testing of futuristic intelligent battle-field sensor networks. In this paper, results are presented for an extensive high-resolution geophysical characterization study at the SWTR site along with validation using 3-D modeling. In this study, several shallow seismic methods and novel processing techniques were used to generate a 3-D grid of earth seismic properties, including compressional (P) and shear (S) body-wave speeds (V_p and V_s), and their associated body-wave attenuation parameters (Q_p, and Q_s). These experiments covered a volume of earth measuring 1500 m by 300 m by 25 m deep (11 million cubic meters), centered on the vehicle test track at the SWTR site. The study has resulted in detailed characterizations of key geophysical properties. To our knowledge, results of this kind have not been previously achieved, nor have the innovative methods developed for this effort been reported elsewhere. In addition to supporting materiel developers with important geophysical information at this test range, the data from this study will be used to validate sophisticated 3-D seismic signature models for moving vehicles.

Each of the four material-property volumes (V_p, V_s, Q_p, and Q_s) was constructed by interpolating 2-D seismic measurements made along survey lines optimized for the physical properties at the SWTR site. The geostatistical properties of the data guided the interpolation of data points between survey lines and established confidence limits around each interpolated value. Ground truth was accomplished through cross-hole seismic measurements and borehole logs. Surface wave and refraction acquisition methods were used to acquire most raw data for this study. In addition to standard reflection and refraction data analysis procedures, we also applied turning ray tomography and surface wave analysis. A variety of seismic energy sources (including vibroseis, accelerated weight drop, and high frequency impulses from projectile and explosive shots) and recording array configurations were considered for optimizing the quality of each analysis.

Inversion of the specific portions of the seismic wavefield was key to the success of the characterization effort. Tomographic inversion produced P-wave velocity matrices with the greatest resolution and finest sampling without the necessity for assumptions about layer properties. Standard refraction analysis was used to confirm the tomographically defined P-wave velocities and to map prominent layers. Inversion of surface-wave dispersion curves from multichannel data resulted in optimal estimates of the S-wave velocity field. Prior to this study, no numerically rigorous methods had been documented for estimating Q for near-surface materials. Geophysical properties at the site appear to be anisotropic, reflecting local trends in near-surface geology. For example, spatial continuity in V_s can be envisioned as an ellipsoid whose semiaxes are 119 m, 95 m, and 9.5 m in length. The longest axis, representing the range of greatest spatial continuity, is oriented W23°N and the shortest axis is vertical. Block kriging was used to estimate averages of geophysical properties within $0.5 \times 0.5 \times 0.5$ m cells and the uncertainties associated with each block in the volume. Weights used in kriging are a function of distance, direction, and rate of spatial

Report Documentation Page

Report Date	Report Type	Dates Covered (from... to)
01OCT2001	N/A	-

Title and Subtitle 3-D Characterization of Seismic Properties at the Smart Weapons Test Range, YPG	**Contract Number**
	Grant Number
	Program Element Number
Author(s)	**Project Number**
	Task Number
	Work Unit Number
Performing Organization Name(s) and Address(es) U.S. Army Corps of Engineers, CRREL 72 Lyme Road Hanover, New Hampshire 03755	**Performing Organization Report Number**
Sponsoring/Monitoring Agency Name(s) and Address(es) Department of the Army, CECOM RDEC Night Vision & Electronic Sensors Directorate AMSEL-RD-NV-D 10221 Burbeck Road Ft. Belvoir, VA 22060-5806	**Sponsor/Monitor's Acronym(s)**
	Sponsor/Monitor's Report Number(s)

Distribution/Availability Statement
Approved for public release, distribution unlimited

Supplementary Notes
Papers from 2001 Meeting of the MSS Specialty Group on Battlefield Acoustic and Seismic Sensing, Magnetic and Electric Field Sensors, Volume 1: Special Session held 23 Oct 2001. See also ADM001434 for whole conference on cd-rom., The original document contains color images.

Abstract

Subject Terms

Report Classification unclassified	**Classification of this page** unclassified
Classification of Abstract unclassified	**Limitation of Abstract** UU

Number of Pages
18

change observed in the data. The noted uncertainties tended to reach their largest values for cells located farthest from measurement points, but rarely exceeded 10% of the estimated values (V_s, V_p, Q_p, and Q_s).

Forward modeling was conducted on the Yuma 3-D model using a 3-D 8th order finite difference scheme that includes topography. The model had a dimension $401 \times 151 \times 51$ cells with 0.5 meter spacing. The time step used was 0.0001 seconds. Due to the size of the model, DoD supercomputers were used in the computation. A vertical point source was used with peak pressure at 0.015 seconds. The elastic (infinite Q) model was computed for reference and to bench mark the attenuation. Results are compared with Yuma field data. After scaling the source magnitude good agreement is found in amplitude, arrival times, amplitude decay rates and frequency spectra of dispersed phases.

1. INTRODUCTION

Development of battlefield sensor networks intended to classify, track, and monitor ground vehicle traffic in forward operation areas will become increasingly critical to the modern Army's intelligence mission. It is expected that these networks will rely heavily on seismic sensing capabilities and must function with a high degree of reliability across a wide range of geologic settings. Discriminating and classifying various types of surface vehicles based on their unique seismic characteristics or signature requires *a priori* knowledge of each target vehicle's characteristics and information about the local near-surface earth properties that influence the propagation of the seismic wavefield. Confidently estimating key near-surface earth material properties in hostile areas will ultimately require interfacing near-surface geophysics and remote sensing technologies. Earth seismic properties are critical components to wavefield simulations and ultimately must be available for incorporation into sensors designed for deployment in areas unavailable for occupation.

Effective seismic sensing technologies deployed in forward operational areas will depend on direct or inferred site-specific knowledge of the earth's physical properties. Wavefield simulations and verification of smart-system performance requires calibration in specific type localities. Such performance evaluations require accurate estimates of real seismic properties in three dimensions, with a level of 3-D detail consistent with site-specific geology and computational constraints. Accuracy and resolution of the methodologies used to extract critical earth seismic properties form the basis for confidence ratings and boundary conditions required to develop procedures for vehicle-type identification from seismic wavefield analysis. Correlation of seismic wavefield models with real seismograms in specific geologic settings provides both the mechanism to quantify the performance of simulations and discrimination algorithms, and the best means to refine various approaches of extracting seismic properties from field seismic wavefield measurements.

Resolution requirements of seismic wavefield propagation models and real earth properties dictate the size and orientation of each grid cell within the specified earth volume. Characteristics of this volume determine the propagation of the modeled seismic wavefield used for quantitative comparisons with field-measured vehicle signature data. By incorporating geostatistical analyses into the estimation of geophysical properties in each cell of the volume, the estimations can be optimized and the estimation process made more efficient. Geostatistics focuses on the rate and direction of changes in geophysical characteristics of the near surface and relates these changes to the spatial arrangement of the sample points. Designing the distribution of cells in the model, interpolating between sample points, and constructing confidence levels for geophysical properties in the 3-D volume is best done using geostatistical procedures**.**

Key seismic propagation parameters, including seismic body-wave velocities (V_p, V_s) and estimates of seismic energy loss in terms of Q_p and Q_s, must be determined for each cell. In addition to these key properties, earth models must also preserve local topographic variation, layer positioning, and thicknesses to be realistic. Since seismic properties can be defined using data acquired via a variety of geophysical

methodologies and approaches, it is necessary to evaluate each to insure the most direct, accurate, expedient, and (laterally and vertically) continuous approach is employed for each unique geologic setting. Evaluations of propagation patterns and the imaging potential of different seismic methods focused on P-and S- body waves (reflected, direct, and refracted) as well as multi-modal surface waves (inversion of dispersive attributes). Estimates of these seismic properties throughout the 3-D earth model can effectively be bounded by geostatistical analyses.

Optimal, and preferably redundant, independent estimates of V_p, V_s, Q_p, and Q_s are necessary for each subsurface cell. Acquiring seismic data using parameters and equipment targeting specific parts of the wavefield permit the most accurate estimation of V_p and V_s. Estimating Q compatible with the rigors of near-surface wavefield modeling has received only scant notice in the published scientific literature (Jeng, et al., 1999). Considering the fundamental dependence of surface wave energy on P- and S- wave characteristics of earth materials, determining Rayleigh wave attenuation as a function of frequency allows estimations of Q for both S- and P-type waves. Extending frequency-dependent attenuation into depth requires innovative approaches to sampling and inversion.

The ability to accurately predict wave propagation in complex geology can have a huge impact on both sensor system development time and expense. Previously, the limiting factor in 3-D seismic wave modeling has been that 3-D representations of geology make the computational task of forward modeling too expensive. Recent leaps in computational power of the supercomputers make this a possibility. While the physics regarding wave propagation is well known, validation of the computer algorithms and the earth model are necessary to make virtual sensor system development on computers a viable option. With validated models there is no limit to model scenarios or sensor placement, making virtual sensor system development a possibility and saving millions of dollars in system development.

Up-stream support of such a virtual sensing system necessitated a set of carefully designed, near-surface geophysical experiments using state-of-the-art high-resolution seismic exploration methods combined with geostatistical analysis techniques to provide essential earth properties for the desert setting of YPG. The primary objective of these experiments was to define 3-D, micro-geophysical variations over a well-defined portion of the SWTR site at YPG. Of particular concern was the mapping the seismic earth properties that most significantly impact the multi-mode propagation of the seismic surface waves.

2. SITE CHARACTERIZATION USING GEOPHYSICS

Historically, when geophysics has been used for site characterization, the attempt involves measurement and incorporation of data from at most two or perhaps three different tools or techniques, each responding differently to different earth properties. Rendering of these data into quantitative information about the geophysical characteristics of the subsurface has generally stopped once first order correlations with specific property changes have been made with “reasonable” confidence. For example, if shallow seismic is one of the tools, interpretations typically have focused on qualitative assessment of subsurface layer topography rather than on quantitative measurements (Clement, et al., 1997; Pullan and Hunter, 1990; Lankston, 1990). The resulting acoustically derived subsurface structure and velocity maps are incorporated into geologic and hydrologic models constructed from borehole data. These simplistic models are then used for groundwater monitoring purposes in an intuitive, experience-based manner (Steeples and Miller, 1990; Miller and Xia, 1999).

Considering the wealth of information contained in the seismic wavefield, seismic measurements or imaging data have been underutilized for site characterization (Steeples, et al., 1995). Surface seismic techniques have been limited almost exclusively to routine mapping and delineation of subsurface structures, layer topography, anomalies, and stratigraphic changes (Jongerius and Helbig, 1988; Miller, et al., 1989; Goforth and Hayward, 1992; Miller, et al., 1995; Shtivelman, et al., 1998; Guo and Liu, 1999; Stokoe,

et al., 1994; Michaels, 1999). In many instances, different earth properties (V_p, V_s, Q_p, Q_s, layer orientations, and thicknesses) could be estimated from different parts of the seismic wave type, providing the potential for redundant measurement if several techniques have been applied coincidently.

3. GEOLOGIC SETTING

YPG is in the Sonoran Desert of the Basin and Range Province in southwestern Arizona (Millet and Barnett, 1970). In general, this area is tectonically characterized by crustal extension that has produced sequences of grabens separating fault-bounded mountains (horsts). These bedrock uplifts (mountains) are separated by broad valleys filled with alluvial and colluvial sediments eroded from those mountains. Sediments that fill the basins have grain sizes that range from clay to boulders. The SWTR site is within the KOFA firing range where the ground surface is characterized by extensive outwash networks separated by fan deposits and areas of desert pavement. The sparse vegetation is mostly clustered around washes.

The ground surface at the SWTR site slopes gently southward with distinct 1 to 2 m high ridges that meander generally north to south across the northern half of the site. Sediment particles within the 0.5 km^2 test area vary in size from gravel to clay, with locations in the site where sorting into distinct surface patches is evident. Geological logs from borings near the center of the SWTR site suggest that the first 100 m of sediment are composed predominantly of silt, gravel, and sand (Jones, 2001). From 0 to 7 m depth, the materials are silt with sand and minor amounts of gravel. Between 7 and 28 m depth, the sediments are mostly gravel with some suggestions of boulders. From 28 to over 65 m depth, the sediments are predominantly silts and sands with minor amounts of gravel.

4. TESTING VARIOUS SEISMIC METHODS

Establishing feasibility and appropriate acquisition design specifications for quantifying the 3-D seismic properties of the test area mandated a unique combination of seismic walkaway testing with geostatistical analyses. Test data were acquired using a 2½-D radial-fan spread configuration, which from a geostatistical perspective best provided estimates of geophysical directionality in the test area (Figure 1). To accommodate the requirements of this novel testing geometry and procedure, constraints on depth of interest, logistical limitations, and practicality issues were also considered when deploying the radial source and receiver array. Data acquired along each of three radial profiles were used to estimate the orientation and extent of spatial continuity of geophysical properties. The radial pattern was aligned with and near the center of the test track at the SWTR site and in close proximity to the test borings (Figure 2). These walkaway noise tests were the basis for determining the accuracy and effectiveness of each seismic method, as well as estimating the optimal orientation and spacing of the seismic array.

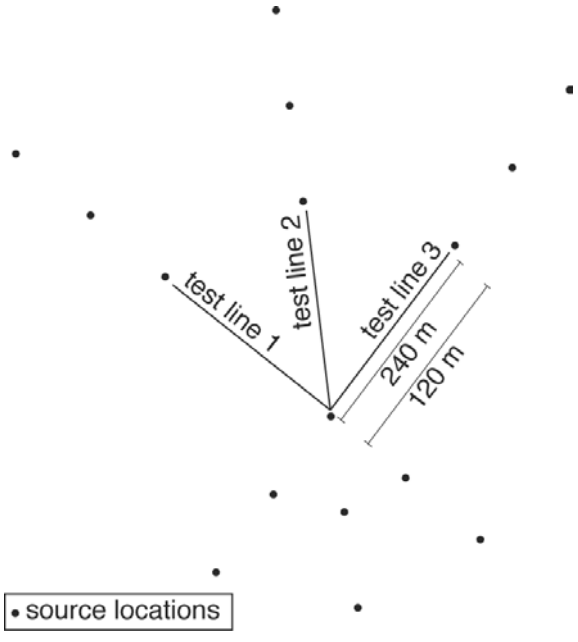

Figure 1. Radial walkaway spread deployed to investigate the antisotropy of geophysical properties at the SWTR site. From a geostatistical perspective this source/receiver configuration best provided estimates of geophysical directionality in the test area.

A variety of sources and receivers was evaluated using this radial spread pattern. Receiver separation for the 240 receivers making up a line in the fan pattern was 0.5 m or 1.0 m (depending of the energy mode being

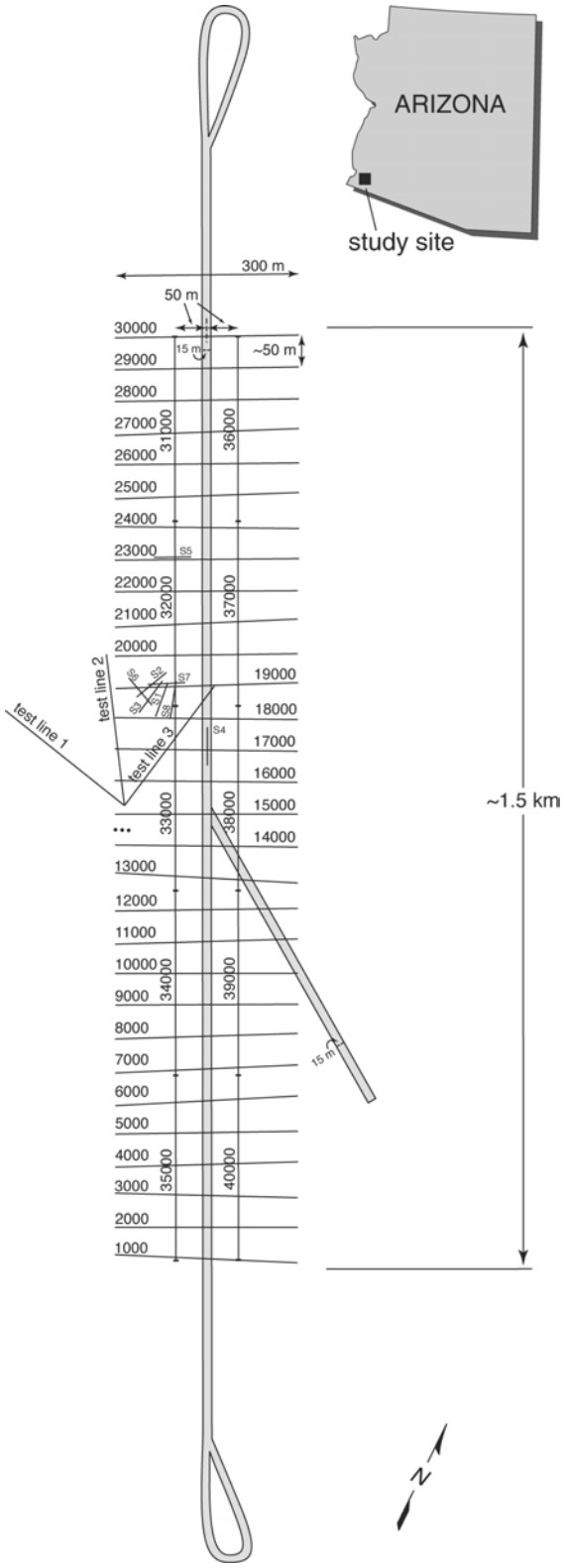

Figure 2. SWTR site relative to the state of Arizona. Profile lines as defined by the high-resolution GPS survey. Relative grid orientations, testing areas, and well locations are identified.

analyzed) with source stations located 240 m, 120 m, and 1 m off each end and centered on the spread. With this configuration all critical offsets and propagation directions could be fully sampled for each source configuration and energy type. Four different receivers were used, depending on the portion of the wavefield being targeted and the dominant mode of seismic waves being generated (14 Hz horizontal, 4.5 Hz vertical, 10 Hz vertical, and 40 Hz vertical). A total of nine different sources was tested at appropriate offsets. These include 20 lb and 12 lb sledgehammers, 12- and 8-gauge downhole shotguns, 30.06 and 50-cal downhole guns, LSS6 land airgun, Rubberband Assisted Weight Drop (RAWD), and IVI minivib.

4.1 Reflection

Analysis of these data for high-resolution P-wave or S-wave seismic reflections using both conventional and high-resolution methods (Steeples and Miller, 1990), as well as adaptations made specifically for these data did not reveal events that could be confidently and consistently interpreted as reflections. Model reflection hyperbolae generated from borehole data were used as templates for evaluating coherent arrival patterns. In light of the extensive testing and analysis of these data, it is unlikely that reflected energy having significant resolution potential has been produced, much less recorded, at this site. The focus of the reflection data acquisition and analysis was the generation and identification of the high-resolution reflections (>100 Hz P-wave and 60 Hz S-wave) necessary for successful use of this method.

4.2 Surface Wave Inversion

Surface waves traditionally have been viewed as noise in multichannel seismic data collected to image targets for shallow engineering, environmental, and groundwater purposes (Steeples and Miller, 1990). Recent advances in the use of surface waves for near-surface imaging combine spectral analysis techniques (SASW), developed for civil engineering applications (Nazarian, et al., 1983), with multitrace reflection technologies developed for near surface (Schepers, 1975) and petroleum applications (Glover, 1959). The combination of these two uniquely different approaches to seismic imaging of the shallow subsurface permits non-invasive estimation of S-wave velocities and delineation of horizontal and vertical

variations in near-surface material properties based on changes in these velocities (MASW) (Park, et al., 1996; Xia, et al., 1999; Park, et al., 1999).

Extending this imaging technology to include lateral variations in lithology as well as tunnel and fracture detection, bedrock mapping, and delineation of subsidence in karst terrains has required a unique approach that incorporates SASW, MASW, and CMP methods. By integrating these techniques, 2-D S-wave velocity profiles of the subsurface can be generated. Estimating the dispersion curve from up to 60 closely spaced receiving channels calculated every 1 to 5 m along the ground surface enhances the signal and results in a unique, relatively continuous view of shallow subsurface S-wave velocity characteristics. This highly redundant method consistently produces S-wave velocity estimates that are within 15% of borehole measurements (Xia, et al., 2000). Continuous oversampling (redundant sampling) of the subsurface minimizes the likelihood that irregularities resulting from erratic dispersion curves or inversion will corrupt the analysis.

Estimates of Q flow naturally from analyses of surface wave attenuation, specifically from Rayleigh wave attenuation (Xia, et al., 2001). Q values for the shallow subsurface were estimated using three related but different approaches (½λ from velocity and $\alpha_r(f)$, single-value average of near-surface layer based on ½λ approximation, and inversion of $\alpha_r(f)$ using V_s derived from MASW), each solving for Q_s and estimating Q_p based on $Q_p \approx 2Q_s$. Inverting $\alpha_r(f)$ to solve for Q_s using V_s derived from MASW is significantly more stable and accurate (reduces error [>25%]) than commonly employed AVO methods (Jin, et al., 2000).

Surface-wave data from the radial test spread were of sufficient bandwidth and signal-to-noise ratio to allow consistent and convergent inversion of dispersion curves to S-wave velocities. Analysis of the test data allowed selection of sources, receivers, and spread/offset ranges optimal for sitewide investigations. Since source, receiver, and spectral requirements for optimal surface wave data were different from those required to collect optimal near-surface reflection data, if both reflection and surface wave methods had provided useful information it would have been necessary to acquire at least two unique data sets along each profile.

4.3 Refraction/Tomography

Direct and refracted P-wave and S-wave arrivals were analyzed using conventional methods (Palmer, 1981; Haeni, 1986; Lankston, 1990) and inversion techniques (Scott, 1977; Schneider, et al., 1992; Ivanov, et al., 2000). Use of direct and refracted arrivals for mapping distinct velocity contrasts between layers has been in routine use for everything from crustal seismic research (Steinhart and Meyer, 1961) to shallow groundwater studies (Haeni, 1978). Well-documented limitations of the technique (Soske, 1954; Sander, 1978) associated with velocity inversions and hidden layers limited refraction analysis at this site. A pronounced velocity inversion in both P- and S-wave borehole measurements at 30 m constrains classic refraction data analysis (Figure 3). Methods exist for approximating solutions when physical

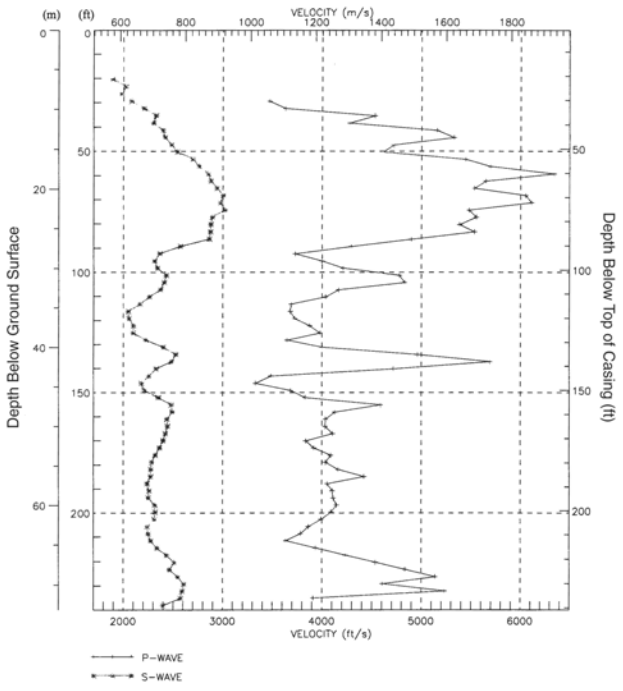

Figure 3. V_p and V_s profiles from the boreholes located at about the mid-way point of the test tract (Figure 2) (Block, 2001). Measurements based on cross-hole configuration.

conditions (such as the velocity inversion observed at the SWTR site) violate assumptions of the refraction method (Mooney 1981; Redpath 1973), but lack the robust nature of tomographic techniques when dealing with these situations.

Tomography has been used to solve many subsurface problems (Peterson et al., 1985; Cottin, et al., 1986; Lytle and Dines, 1980; Kilty and Lange, 1990). A tomographic technique (Joint Analysis of Surface Waves and Refraction [JASR]) incorporating inversion of first arrivals with an initial model from S-wave velocity profiles from surface wave data (Ivanov, et al., 2000) provided 2-D V_p sections consistent with borehole measurements. The simplicity of acquisition and computations made tomographic analysis especially attractive for velocity estimation using data optimally acquired for surface-wave analyses. Perhaps equally important is the inherent subdivision of the earth into cells, fundamental to tomographic analysis. A true advantage to the JASR method used here is its ability to overcome the non-uniqueness problem inherent in conventional refraction and refraction tomography methods (Ivanov, et al., 2000). This approach increases the detail in resulting images and therefore improves the apparent resolution, and since calculations of V_p are based on a cellular approach, correlations with the V_s grid cells calculated by MASW are straightforward.

First arrival analysis of the radial pattern walkaway test data was limited to the upper 30 m and produced a two-layer V_p model using conventional refraction methods and a 10-layer V_p cell model using the JASR method. The continuity in transitions between layers inherent in tomographic analysis provides a more meaningful cross-section for incorporation into grid cells containing other seismic properties. Both V_p models were produced for the sitewide 2½-D grid, but only the JASR data were incorporated into the wavefield simulations. Secondary analysis of the radial pattern walkaway data indicated that parameters and equipment used to optimally acquire surface wave data for the SWTR site were well within the tolerances for both conventional refraction and JASP first arrival analysis. Using the same data set for several analyses minimized the field data collection effort and enhanced the consistency in estimates of different seismic properties for each cell.

5. GEOSTATISTICAL ANALYSIS AND GRID DESIGN

A major objective of the walkaway test was to determine if there were significant anisotropies in geophysical properties at the test site, possibly as a result of local trends in the geology. The radial design of the seismic lines provided measurements of geophysical properties along three different orientations. By computing the semivariance along these three lines, a directional estimate of the range of a geophysical property such as V_p could be made. (The *range* defines the spatial limit of partial dependence between observations; beyond the range, observations are statistically independent and values at one location are unrelated to values at other locations which lie beyond the range.) In three dimensions, the range can be envisioned as an ellipsoidal envelope. The three walkaway lines can be regarded as vectors extending from the center of the ellipsoid to the margins of the envelope. The direction cosines of the vectors express the orientations of the walkaway lines and their lengths are proportional to the ranges of the geophysical properties along the lines. These relationships can be expressed in a 3×3 matrix whose eigenvalues and eigenvectors represent the major and minor axes of the envelope, and which define the direction and extent of anisotropy. At the SWTR site, the direction having the greatest range is oriented N23°W with a range of 118.9 m. The range in the perpendicular direction is 95.1 m. The range in the vertical direction is 9.5 m. These properties allow the design of an optimal sampling grid for the main phase of data collection.

The sampling plan used at the SWTR site consists of parallel lines oriented in the direction of most rapid change in geophysical properties. Observations collected along these lines have the greatest sampling density (1.2 m) in the direction of most rapid change in seismic properties. The spacing between lines (50 m) is much greater, but seismic properties are more persistent in this direction. The line spacing of

50 m is such that there is complete overlap in range from one line to the next, so every estimated location within the array is partially related to at least two seismic lines. Either through good fortune or foresight by the designers of the SWTR site, the direction of maximum range in geophysical properties is approximately parallel to the test track, which greatly eased the layout of the seismic array.

6. ACQUISITION OF 2½-D GRID

Geophysical and geostatistical analyses of walkaway test data using seismic velocities measured from cross-hole studies for control formed the basis for selecting optimal sources and receivers, source and receiver spacings, line spacings, and the orientation of the major axis of the 2½-D rectangular array. The primary motivation for the radial walkaway test was to allow examination of a wide range of methods and equipment to determine the optimum parameters and survey design, based on geostatistical and geophysical evaluations.

After geostatistical analysis of the radial test data, a 2½-D grid with the long axis oriented parallel to the test track was determined to be optimum for local geologic conditions (Figure 2). Inline spacing of geophones was 1.2 m with short axis lines 300 m long and separated by 50 m. Tie lines were separated by 100 m, parallel to the test track, and 50 m offset from the center of the 300 m spreads and test track. This 40-spread configuration resulted in a uniform 2½-D grid within the 1.5 km by 300 m study area.

The data acquisition program was simplified when high-resolution reflection was dropped from consideration as an effective tool for imaging acoustic impedance contrasts at depths less than 30 m at this site. With first arrival body waves and surface waves left as the only seismic energy types available to exploit at this site, the data acquisition requirements were reduced enough to permit recording a single data set optimized for both analyses.

At most sites where MASW has been effectively used, low natural frequency geophones (4.5 Hz) have provided the best low frequency response while retaining sufficient high frequency components of the surface wave energy to produce a broadband signal. At the SWTR site, triple 10 Hz geophones provided the best response for the depth range of interest. Additionally, these geophones responded well enough to first arrival body wave energy for automatic first-break picking routines to operate efficiently. Optimal source configurations for use in refraction tomography are for the most part similar to those employed in surface wave recording. It is generally preferred to have sources that are high energy producers with a broadband signal centered toward the lower portion of the conventional seismic spectra. The RAWD provided a broad bandwidth and high-energy pulse that produced a very repeatable waveform.

To insure that sufficient offsets were recorded for refraction tomography and that close trace spacing was maintained for MASW analysis, a fixed spread of 240 receiver stations spaced at 1.2 m was deployed for each 300 m profile (Figure 4). A 240-channel Geometrics StrataView seismograph was used to record these fixed-spread data using a source spacing of 4.8 m inline and 1.2 m offline. Each source location was conditioned with an initial unrecorded impact to seat the plate, followed by three recorded impacts. Since the optimum offset window for surface wave sampling of the upper 30 m at this site is between 2 and 25 m, the 240 channel spread can easily be split into appropriate uniform gathers. Quality control was maintained through inspection of each shot gather for signal-to-noise and first break quality. Unacceptable shots were deleted and re-recorded.

High-resolution elevation data were acquired with accuracy better than 8 cm (X, Y, Z). This level of spatial accuracy was critical during the assignment of values to cells within the study volume. If future vehicle tests are performed at SWTR, these spatial data will provide the necessary link between the earth properties and sensor deployments.

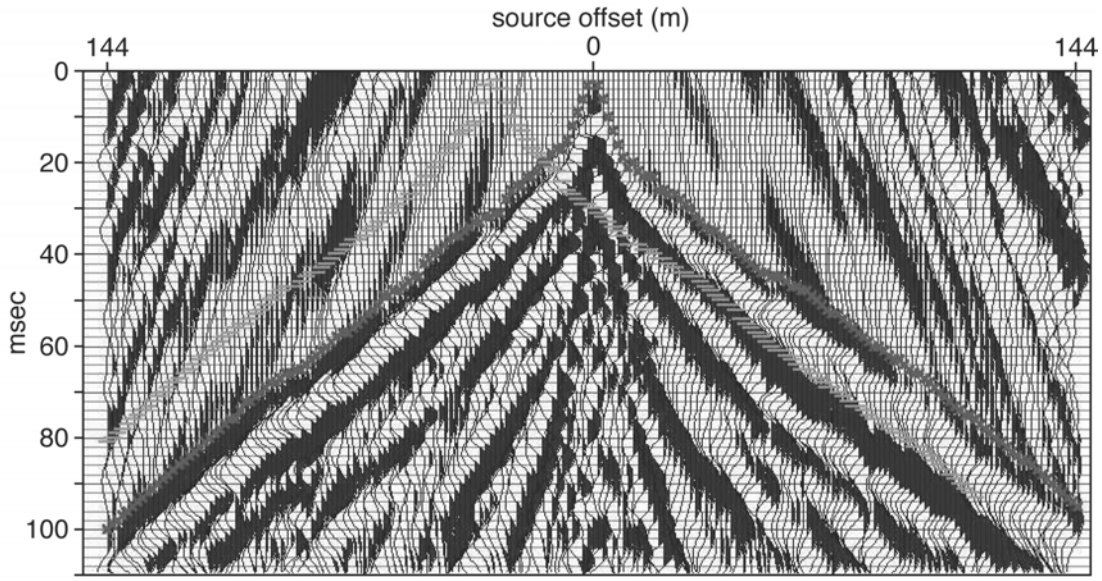

Figure 4. Raw shot gather with first arrival picks from current and previous shot superimposed on section. Low velocity noise arrivals at times prior to the first arrivals are from the engine of the weight drop source.

7. PROCESSING OF 2½-D GRID

7.1 V_s Using MASW

Each 240-trace shot gather was split into a left and right spread. The optimum 60 traces were retained to create consistent offset-distribution shot gathers necessary for best results during MASW processing. These 60 trace gathers were analyzed with SurfSeis (a proprietary software package from the Kansas Geological Survey that facilitates use of MASW for continuous profiling). Each shot gather generated one dispersion curve, which was assigned a surface location corresponding to the middle point of the spread being analyzed (Figure 5). Care was taken to insure that the spectral properties of the t-x data (shot gathers) were consistent with the maximum and minimum f-v_c values (v_c is the phase velocity of surface waves) contained in the dispersion curve.

SWTR data are an exception to the general "rule of thumb" that suggests most Rayleigh wave energy is contained in the fundamental mode. Instead, higher mode Rayleigh wave energy dominates the surface wave frequency band on most shot records. A variety of unique processing steps was undertaken to eliminate higher mode as well as body wave energy. A two-phase dispersion curve analysis routine, requiring extraction of the fundamental mode portion of the dispersion curve and then supplementing this with higher frequency portions of the fundamental mode that remain after time domain muting, provides two dispersion curves with minimal overlap in the frequency domain. These two curves were digitally sutured with each combined dispersion curve individually inverted into an x-vs-z trace. In general, the combined dispersion curves possess a useable bandwidth from about 9 Hz to 65 Hz. Gathering all x-vs-z traces into shot-station sequential order creates a 2-D grid of the S-wave velocity field.

To increase the signal-to-noise ratio and to improve convergence during inversion, a new technique called Filtering of Dispersive Seismic Event (FDSE) was used to suppress higher modes on some shot records. This method removes higher modes through filtering in the frequency domain and avoids the detrimental artifacts that are observed in dispersion analysis if higher modes are removed using time domain muting. Because SurfSeis was designed to invert fundamental mode Rayleigh wave energy only, inclusion of higher mode or body wave energy can inhibit convergence.

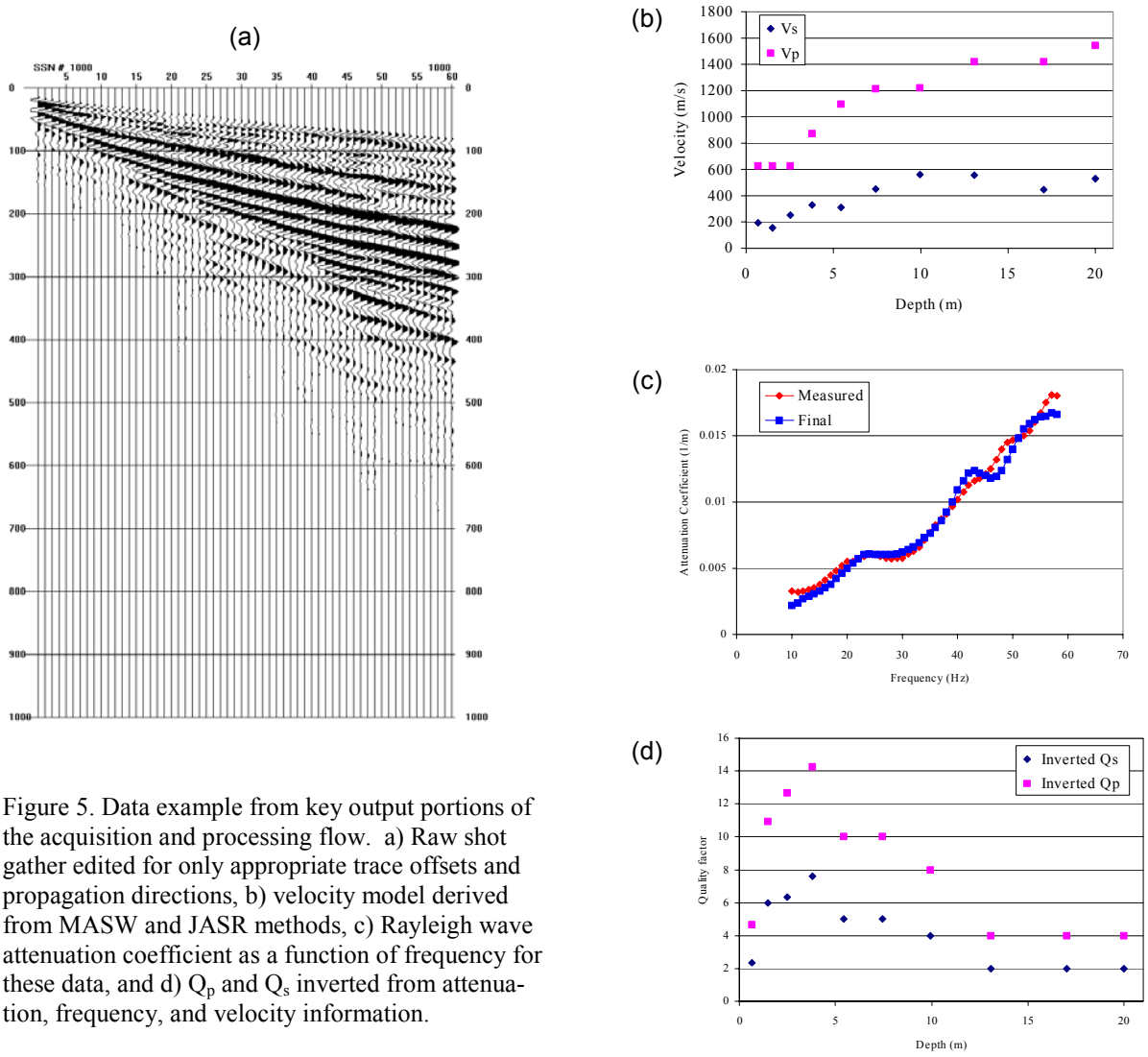

Figure 5. Data example from key output portions of the acquisition and processing flow. a) Raw shot gather edited for only appropriate trace offsets and propagation directions, b) velocity model derived from MASW and JASR methods, c) Rayleigh wave attenuation coefficient as a function of frequency for these data, and d) Q_p and Q_s inverted from attenuation, frequency, and velocity information.

7.2 V_p Using JASR

Considering the resolution requirements and redundancy in rays penetrating each 3 m x 3 m x 3 m cell, first arrivals were picked for all 240 traces on every fifth shot gather. As a result, 17 shot stations produced the V_p cross-section for each line. Supplemental analyses demonstrated that only minor improvements were observed (< 10%) when the number of shots processed per line was increased to 63. As expected, these improvements were due mainly to greater ray coverage. However, dropping the number of shots by as few as two (down to 15) produced noticeable declines in data uniformity and increased the artifacts associated with undersampling. Ray tracing clearly demonstrated the effect of the sampling distribution within the volume in general, and the effect that each cell had on the final velocity profile (Figure 6).

Two-dimensional V_s cross-sections obtained from MASW analysis were used to generate an initial inversion model for the tomographic inversion to V_p (Ivanov, et al., 2000). The initial model was optimized by iterating the estimate of Poisson's ratio until the first arrivals predicted from modeling correlated with the actual shot records. Several inversion runs were made using the initial model to converge on conditioning

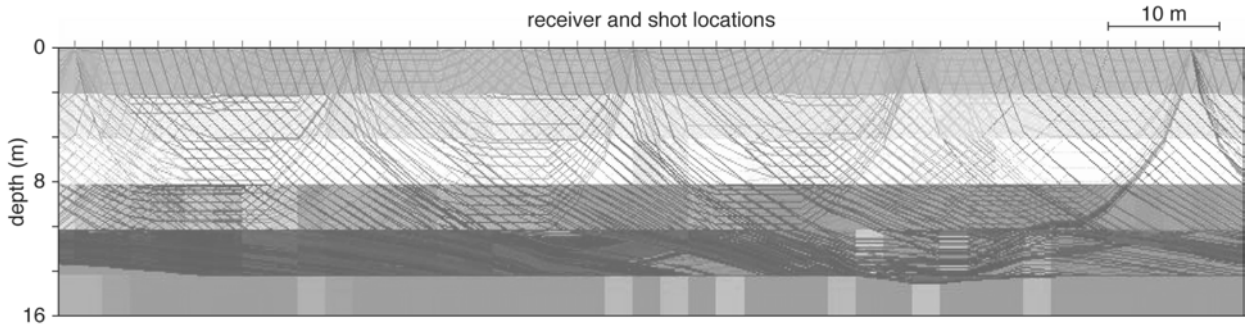

Figure 6. Ray tracing from tomographic analysis of first arrival data. High concentrations of rays penetrate all layers of the model. Especially, high densities can be observed through layer 5 of this model.

parameters appropriate for this data set. Fine-tuning of the initial model is optimized when best-fit conditioning parameters were used during preliminary analyses.

By analyzing the correlations between the model and observed data the final inversion process could be used for quality control of the first arrival picking routines. In some instances, secondary first arrival analysis was necessary to converge on a "good" solution. Additional quality control was achieved by verifying that the 2-D V_p/V_s data were reasonable.

7.3 Q

Estimates of Q presented in this paper are enhanced developments based on initial work described by Xia, et al. (2001) and unpublished extensions of that work by Xia et al. Processing these data to obtain Q involved two major steps for the first two methods (λ from velocity and $\alpha_r(f)$ and single value average of near-surface layer based on λ approximation with calculation of Q based on Eq. A3). The third method, inversion of Q from $\alpha_r(f)$, is based on Eqs. A4 through A7 (Appendix A). Consistent with other estimations of Q in the shallow subsurface, Q decreased with depth. Q has been demonstrated to have a wide range of responses to increases in depth for various geologic settings (Xia, et al., 2001). Intuitively, increasing depth should increase the quality factor which then relates to decreases in attenuation. However, regardless of the method used to calculate Q it consistently decreased with depth in the upper 30 m at this site. Decreases in Q estimates observed when using approximation methods were the basis for development of the three-method approach to defining Q as a function of depth necessary for model simulations. More extensive and detailed model simulations will eventually provide the best verification for these observations.

8. GEOSTATISTICAL PROCESSING OF V_p, V_s, Q_p, AND Q_s

Conventional statistics assumes that observations used in estimation are independent; that is, the value of one observation has no influence on the value of a subsequent observation. This assumption is not valid for many natural phenomena such as geophysical properties, because a value at one location obviously is related to values at nearby locations and less closely related to values at more distant locations. *Geostatistics* is a special branch of applied statistics that takes advantage of the spatial dependence between samples distributed in space to produce optimal estimates of a property at unsampled locations, and to assess the error associated with these estimates. Although the geostatistical literature is vast, there have been relatively few applications in geophysics. An introduction to geostatistics is given by Davis (2002) and a thorough treatment is provided by Olea (1999) and, from a statistical viewpoint, by Cressie (1993).

Information on spatial continuity is derived from a model of the *semivariogram*, a function that relates distance between observations to the mean difference between observations. The model is fitted by weighted least squares or similar procedures to empirical values of semivariance that are calculated from the observations. For a property that is spatially stationary, the semivariance is inversely proportional to the autocorrelation between observations. A theoretical semivariogram (model) is used rather than the observed empirical semivariogram because the semivariances must be evaluated for any distance, not just the discrete distances between observations (Figure 7).

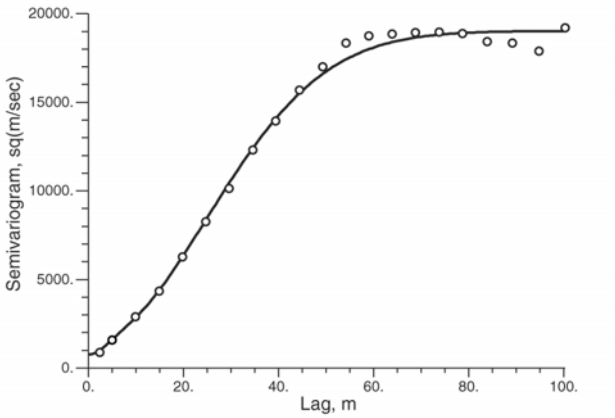

Figure 7. Semivariogram of V_s computed along seismic lines in the SWTR site, YPG. Open circles are calculated semivariances; fitted line is a best-fit model (nested Gaussian model with a range of 60.7 m).

The estimator used in geostatistics is *kriging*, a family of generalized linear regression techniques in which the value of a property at an unsampled location is estimated from measured values at neighboring locations. Kriging estimates require prior knowledge in the form of a model of the semivariogram or the spatial covariance. Kriging differs from classical linear regression in that it does not assume that variants are independent, nor does it assume that observations are a random sample.

Kriging is used to make regular two- or three-dimensional grids of estimates of geophysical properties, which constitute the required earth model. Unlike conventional gridding algorithms, kriging produces grids that have statistically optimal properties. Kriging is an exact interpolator; that is, values estimated by kriging will be exactly the same as the observations at the same locations. Kriging estimates are unbiased, so the expected value of the estimates is the same as the expected value of the observations. Perhaps most importantly, the error variances of kriging estimates are the minimum possible of any linear estimation method, and the error variances can be estimated at every location where a kriging estimate is made. This provides a way of expressing the uncertainty of a property. The kriging estimates, in combination with the estimation variances, can be interpreted as "lowest likely" values, "most likely" values, and "highest likely" values of the geophysical property at every location within the model volume.

In general, a kriging estimate at location 0 is given by $\hat{Z}_0 = \mathbf{Y}'\mathbf{W}^{-1}\mathbf{B}$ and the kriging estimation error variance is $\sigma_0 = \mathbf{B}'\mathbf{W}^{-1}\mathbf{B}$, where **Y** is a vector of the observations used in the estimate, **W** is a matrix of semivariances between these observations, and **B** is a vector of semivariances corresponding to the distances between the observations and the location being where the estimate is to be made. The appropriate form of estimation used in this project is *block kriging,* the general name for a collection of kriging procedures that include a change from point observations to estimates that represent the average of volumes. Olea (1999) provides a succinct development of block kriging, and a less formal discussion is given by Isaaks and Srivastava (1989). In block kriging, the right-hand vector **B** represents the averages of semivariances between the point observations x_i and all possible points within *A*, a volume of interest. (Actually, the elements of the right-hand vector **B** represent the semivariances between the observations and *A*, integrated over the volume of *A*. As a practical matter, the integration must be approximated by averages of semivariances between the observations and point locations within *A*.) Typically, determining the kriging estimate and estimation variance for one block requires solving a set of 32 simultaneous equations. Each earth model based on the first 15 lines at the SWTR site contains 30,468,381 blocks or cells. There are two parts to each model, one containing an estimate of a geophysical property such as V_p in each cell, and the other containing the estimation variance for each cell. Models have been prepared for eight geophysical properties, plus a 2-D model of surface topography.

To produce the earth model of a geophysical property such as V_s (Figure 8), we first compute directional semivariograms and examine them for nonstationarity. If nonstationarity is detected, semivariogram models are computed in a direction perpendicular to the drift and used for block kriging. This insures that a conservative set of observations will be used in calculating the kriging estimates. A series of experimental models are fitted to the experimental semivariances and the model producing the smallest estimation error is chosen. This semivariogram model is then used to produce block kriging estimates for the geophysical property. A cross-validation is performed to verify that the block kriging estimates are valid and that the observed estimation errors are within the theoretical limits. The resulting three-dimensional solid model can be displayed as cross-sections along any desired row or column, and as maps of any desired layer.

The results of geostatistical analyses can be provided in the form of conditional stochastic realizations (Deutsch and Journel, 1998). Each realization is a three-dimensional array whose values conform exactly to the observed data at every control point along the seismic lines. At all interpolated locations, the values will follow the same statistical distributions as the observed data. Each realization is a "possible scenario" which has characteristics that are statistically identical to those actually observed. These stochastic alternatives can be used to evaluate the simulation model to determine the model's sensitivity to variation in geological and geophysical properties.

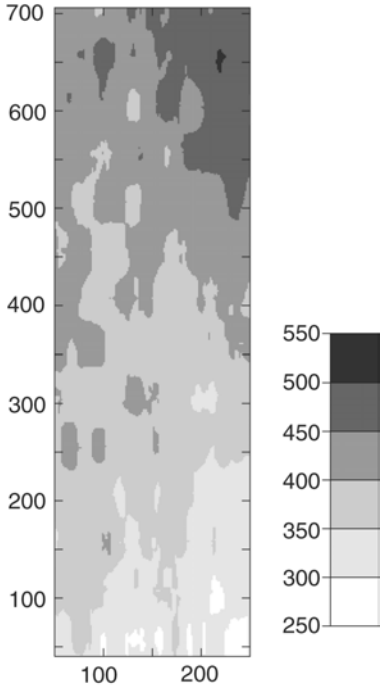

Figure 8. Shaded contour map of V_s at 5 m depth, SWTR site, YPG. Map coordinates are in meters from an origin at the southwest corner; contour interval is 50 m/sec.

9. SIMULATIONS USING 3-D VOLUMES OF V_p, V_s, Q_p, AND Q_s

Simulations of wave propagation through a KGS Yuma earth model were performed using a 3-D 8th order finite difference staggered grid scheme (Ptop) and directly compared to field data. The combined variations in geophysical parameters and topography in three dimensions make seismic wave propagation a highly complex phenomenon. Successful synthetic comparisons with field data give both validation of the Ptop code and demonstrate the consistency of geologic characterization.

The preliminary 3-D KGS Yuma model had a dimension of 401 x 151 x 51 nodes with 0.5 meter spacing. The parameters provided by KGS were V_s, V_p, Q_s, Q_p, rho, and elevation. A three-dimensional view of V_s is plotted in Figure 9. The Ptop finite difference code allows a non-planar surface (Hestholm, 1999) and therefore the elevation data (Figure 10) was incorporated into the model.

The anelastic (Q) implementation of Ptop required relaxation time constants to be calculated. It was necessary to reduce the

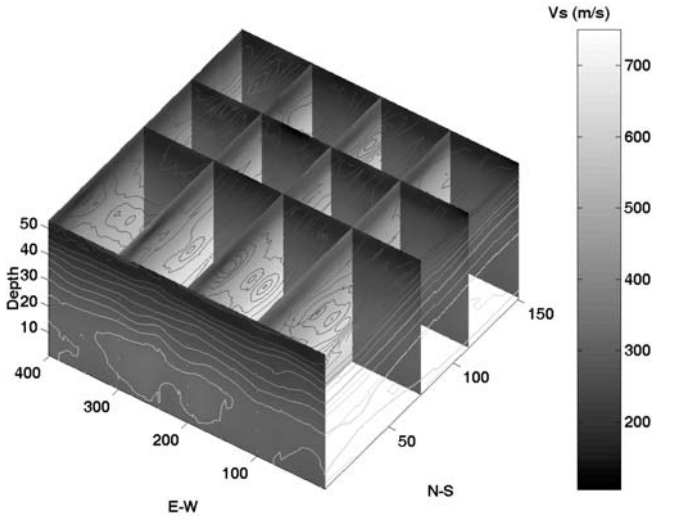

Figure 9. KGS 3-D S-wave velocity used in finite difference calculations.

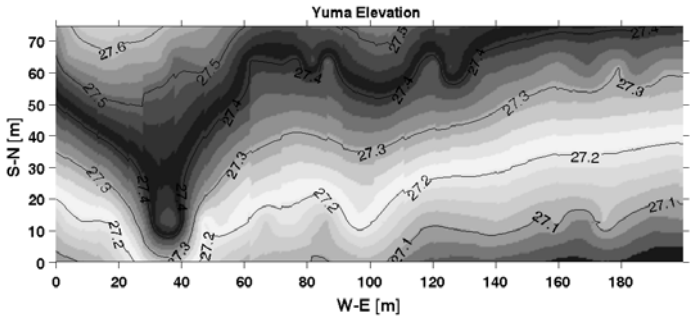

Figure 10. KGS 3-D surface elevation used in finite difference calculations.

computation for constants from 401 x 151 x 51 x n, where n is the number of relaxation mechanisms, to a more reasonable number. The data set was simplified by rounding velocities to the nearest tens of m/s and binning accordingly. Model parameters were grouped and assigned to a representative unique velocity block, in this case 91 unique S-wave velocities. This reduced computation for Q relaxation parameters to 91 x n. Computations for both the elastic and anelastic models were run.

The time domain traces were normalized on the maximum amplitude of each trace to emphasize waveform characteristics, arrival times, and illustrate the relative size of the fundamental mode, the particular phase of interest. Time domain plots of the normalized velocity amplitudes for the anelastic case and field data are shown in Figure 11. The synthetics predict accurate arrival times for both the P and surface waves out to 100 meters. The relative amplitude of the fundamental mode to the P arrival is consistent with the data. The ringing of the surface wave seen in the field data is not reproduced in the synthetics. This may be due to fine near surface layering (less than 2 meter) where the model is poorly constrained or to complexity in the source where weight bouncing may be occurring.

The amplitude decay with distance emphasizes the agreement of signal attenuation with distance (Figure 12). Field data was normalized to the Ptop Q synthetic at the 16th receiver (approximately 20 m). This was approximately the range where the clipping of field data stopped. The predicted decay rate from the synthetics agrees well with the decay of the field data. It is noted that the Yuma Q model used here increases with depth.

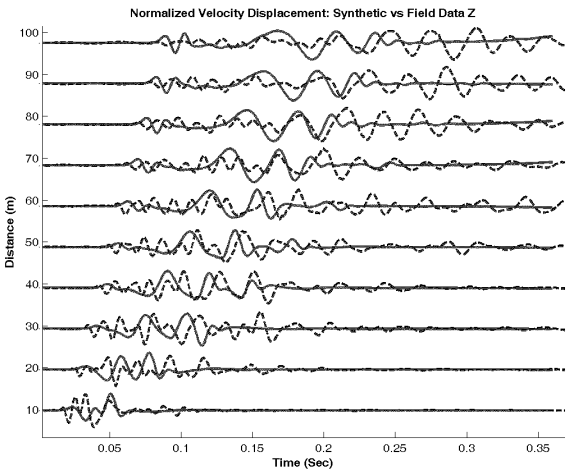

Figure 11. Record section of Ptop synthetics (solid) vs. field data. The fundamental features of P-wave and surface wave arrival times and relative amplitude agree well.

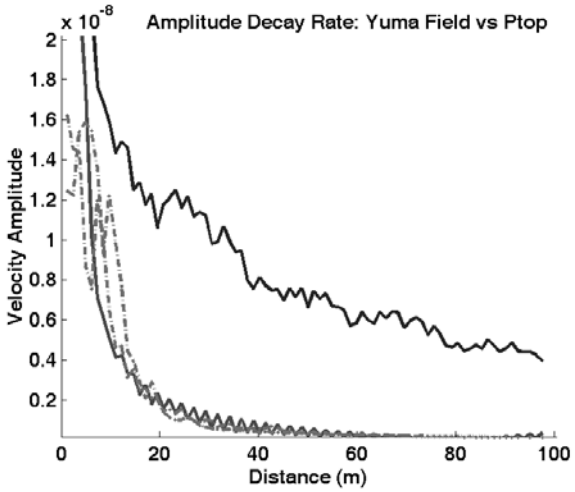

Figure 12. Amplitude decay vs. distance. Ptop synthetics (solid) vs. field data. Synthetic calculated with Q is normalized with field data at approximately 20 m due to clipping. Elastic synthetic decay rate is plotted for reference.

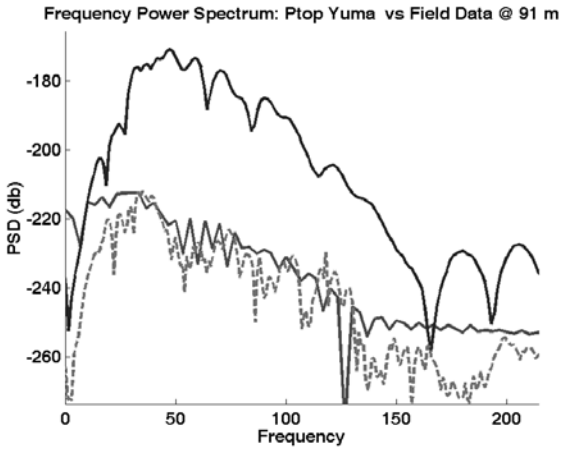

Figure 13. Frequency spectrum for receiver at 91.4 meters. Field data is normalized on maximum of synthetic computed with Q. Spectral content and slope match for 30-110 Hz. The top trace is the elastic synthetic result plotted for reference.

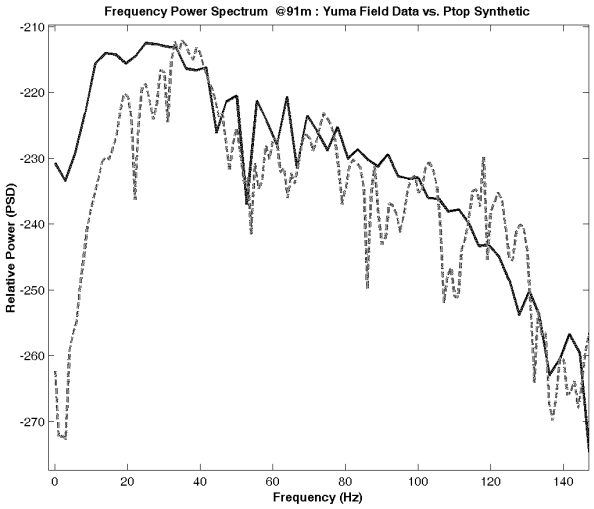

Figure 14. Spectrum of field data and synthetic at 91 m. Synthetic uses Q of Yuma model and includes instrument response.

Finally, to validate the frequency content of the synthetics, the spectra from receivers at 91 meters are plotted in Figures 13 and 14. The spectra are plotted on the same scale, however the field data is normalized on the peak amplitude of the spectra generated by the Yuma Q model. This peak frequency corresponds to the fundamental mode. The implementation of Q severely attenuates the signal, providing peak frequency match as well as the slope of the amplitude from 30-110 Hz. The low frequency amplitude that tapers off in the field data due to instrument response is addressed by convolving the instrument response with the synthetic signal (Figure 14). The synthetic still has more low frequency content than the field data, but the amplitude does drop off sharply at 10 Hz. The slope and content of the synthetic spectra match field data from 30 to 110 Hz. There is also somewhat of a spectral hole at 55 Hz that is matched by the synthetic data. The maximum spectral power at 30-45 Hz in both the field data and the synthetic data corresponds with the fundamental mode or Rayleigh wave.

The quality of agreement is extraordinary and rarely achieved in practice. This is due to the fidelity of the geologic model and the successful Yuma site characterization performed by the KGS/KU.

10. CONCLUSIONS

A high-resolution geophysical characterization of the SWTR site at Yuma Proving Ground in Arizona was performed by the KGS. This data set provides valuable insight into subsurface features that may affect future tests that rely on seismic wave propagation (such as unattended ground sensors). By putting constraints on subsurface heterogeneities and surface topography, a more complete understanding of local wave propagation may be achieved leading to sensor system development and optimization.

Synthetics from the Yuma model with Q predict the amplitude, dispersion and distribution of energy in the frequency domain observed in field data. The agreement is a preliminary validation of finite difference code developed at ERDC-CRREL. The good correlation of Ptop synthetics with field data using simple sources bodes well for future applications where more complex sources are to be used. The ability to predict accurate seismic velocity field displacement is key to relying on synthetic data for sensor system development and optimization. Reliable synthetic data will dramatically reduce system development time and cost.

11. APPENDIX A

Consistent with all three was the calculation of the attenuation coefficient as a function of frequency α_f. The attenuation coefficient is defined by the following expression:

$$A (x + dx) = A (x) e^{-adx}. \quad \text{(A1)}$$

Rayleigh wave amplitude is A, α is the Rayleigh wave attenuation coefficient, and x and dx are geophone location and station interval, respectively. After the FFT with respect to time, the expression becomes:

$$\alpha_f = -\frac{ln\left[\left|\frac{W(x+dx,f)}{W(x,f)}\right|\sqrt{\frac{x+dx}{x}}\right]}{dx}. \quad \text{(A2)}$$

Where α_f is the Rayleigh wave attenuation coefficient as a function of frequency f and W is the amplitude at a specific frequency.

After calculation of α_f, the processing flow diverges for each of the three methods. The first two methods are based on the assumption of a homogeneous medium. The third method is based on a layered earth model. First, ½λ from velocity and α_f requires dispersion analysis to establish phase velocity of the Rayleigh wave relative to frequency. Calculation of Q(f) then follows the relationship:

$$Q(f) = \frac{\pi f}{V_r \alpha_f} \quad \text{(A3)}$$

where V_r is the Rayleigh wave phase velocity as a function of frequency. Moving from Q(f) to Q(z) requires V_r and the ½λ axiom which defines the surface wave's depth sensitivity to elastic module. Q(z) in this case is approximately equivalent to $Q_s(z)$ and ½$Q_p(z)$.

Second is the assignment of a single Q for each surface shot station. This method follows the previous flow for the ½λ approximation method except Q(f) is averaged for all frequencies of interest, providing a single Q_s and Q_p (based on the ½ relationship to Q_s) for each source station.

Finally, by inverting α_f, Q can be estimated. The relationship between Rayleigh wave attenuation coefficients and the quality factors for compressional and shear waves were given by Anderson et al. (1965) as:

$$\alpha_r(f) = \frac{\pi f}{C_r^2(f)}\left[\sum_{i=1}^{n} P_i(f) Q_{pi}^{-1} + \sum_{i=1}^{n} S_i(f) Q_{si}^{-1}\right]. \quad \text{(A4)}$$

where

$$P_i(f) = V_{pi}\frac{\partial C_r(f)}{\partial V_{pi}}, \quad \text{(A5)}$$

$$S_i(f) = V_{si}\frac{\partial C_r(f)}{\partial V_{si}}, \quad \text{(A6)}$$

$\alpha_R(f)$ is Rayleigh wave attenuation coefficients in 1/length, and f is frequency in Hz. Q_{pi} and Q_{si} are the quality factors for compressional and shear waves of the ith layer, respectively. V_{pi} and V_{si} are the P-wave velocity and S-wave velocity of the ith layer, respectively. C_r is Rayleigh wave phase velocity. n is the number of layers of a layered earth model.

Modifying an algorithms discussed in Menke (1984) with a damping factor, it becomes possible to invert for Q using the following statement for $x_i > 0$:

$$A\vec{X} = \vec{B} \quad \text{(A7)}$$

where $\vec{X}$ is the inverse of quality factors (model vector 1/Q), x_i is the ith component; $\vec{B}$ is attenuation coefficients (data vector α); and A is the coefficient matrix determined by equation (4).

Figure 1. Radial walkaway spread deployed to investigate the antisotropy of geophysical properties at the SWTR site. From a geostatistical perspective this source/receiver configuration best provided estimates of geophysical directionality in the test area.

12. ACKNOWLEDGMENTS

This work was supported by the U.S. Army Office of the Program Manager for Mines, Countermines, and Demolitions in support of Hornet, Raptor, and Rattler-Track3 and by the U.S. Army Corps of Engineers, Engineering Research and Development Center, Cold Regions Research and Engineering Laboratory (ERDC-CRREL) under PE62784/AT42. Work at the University of Kansas and the Kansas Geological Survey was by contract DACA42-00-C-0054 with ERDC-CRREL. We would like to extend our appreciation and sincere thanks to the following people for outstanding contributions to this project: Joe Anderson (field assistance and GPS data acquisition); Brett Bennett (GPS data acquisition and processing), Mary Brohammer (manuscript preparation); Mitch Fiedler, Chad Gratton, and David Laflen (field assistance and equipment management); David Fisk (project coordination and field assistance); Ricardo Olea (geostatistical data computations); Choon Park, and Julian Ivanov (geophysical data processing and/or technique development); Chris Tapie (field assistance and geophysical data processing) and Alan Tinseth (site logistics and coordination with YPG).

13. REFERENCES

Anderson, D.L., Ben-Menahem, A., and Archambeau, C.B., 1965, Attenuation of seismic energy in upper mentle: J. Geophys. Res., v. 70, p. 1441-1448.

Block, L., 2001, Crosshole seismic surveys and geophysical borehole logging at the Smart Weapons Test Range, Yuma Proving Ground, Arizona: U.S. Department of the Interior, Bureau of Reclamation, Technical Memorandum No. D8330-2001-10.

Clement, W.P., S. Cardimona, A.L. Endres, K. Kadinsky-Cade, 1997, Site characterization at the Groundwater Remediation Field Laboratory: The Leading Edge, v. 16, p. 1617-1621.

Cottin, J.F., P. Deletie, H. Jacquet-Francillon, J. Lakshmanan, Y. Lemoine, and M. Sanchez, 1986, Curved ray seismic tomography–Application to the Grand Etang Dam (Reunion Island): First Break, v. 4, no. 7, p. 25-30.

Cressie, N.A.C., 1991, Statistics for Spatial Data: John Wiley & Sons, Inc., New York, 900 p.

Davis, J.C., 2002, Statistics and Data Analysis in Geology, 3rd ed.: John Wiley, Inc., New York, 639 p. (in press).

Deutsch, C.V., and A.G. Journel, 1998, GSLIB, Geostatistical software library and user's guide: Oxford Univ. Press, New York, 369 p., 1 CD-ROM.

Glover, R.H., 1959, Techniques used in interpreting seismic data in Kansas: In Symposium on Geophysics in Kansas, ed. W.W. Hambleton. Kansas Geological Survey Bulletin 137, p. 225-240.

Goforth, T., and C. Hayward, 1992, Seismic reflection investigations of a bedrock surface buried under alluvium: Geophysics, v. 57, p. 1217-1227.

Guo, T., and L. Liu, 1999, Non-intrusive evaluation of submarine tunnel foundation using dynamic high-frequency surface wave prospecting: Proceedings of the Symposium on the Application of Geophysics to Engineering and Environmental Problems (SAGEEP 1999), Oakland, Calif., March 14-18, p. 67-74.

Haeni, F.P., 1978, Computer modeling of ground-water availability in the Pootatuck River valley, Newtown, Connecticut, with a section on quality of water by Elinor H. Handman: U.S. Geological Survey Water Resources Investigations Open-file Report 83-4221.

Haeni, F.P., 1986, Application of seismic refraction methods in groundwater modeling studies in New England: Geophysics, v. 51, p. 236-249.

Hestholm, S., 1999, Three-dimensional finite difference viscoelastic wave modeling including surface topography: Geophys. J. Int., v 139, p. 852-878.

Isaaks, E.H., and Srivastava, R.M., 1989, An Introduction to Applied Geostatistics: Oxford University Press, Inc., New York, 561 p.

Ivanov, J.M., C.B. Park, R.D. Miller, and J. Xia, 2000, Mapping Poisson's ratio of unconsolidated materials from a joint analysis of surface-wave and refraction events: Proceedings of the Symposium on the Application of Geophysics to Engineering and Environmental Problems (SAGEEP 2000), Arlington, Va., February 20-24.

Jeng, et al., 1999, An improved method of determining near-surface Q: Geophysics, v. 64, p. 1608-1617.

Jin, S., Cambois, G., and Vuilermoz, C., 2000, Shear-wave velocity and density estimation from PS-wave AVO analysis: Application to an OBS dataset from the North Sea: *Geophysics*, v. 65, p. 1446-1454.

Jones, K.A., 2001, U.S. Army Corps of Engineers Memorandum CEMVK-ED-GI (1110-2-1150a), Trip Report, Yuma Proving Ground near Yuma, Arizona; with attached geologic log and grain size distribution test reports.

Jongerius, P., and K. Helbig, 1988, Onshore high-resolution seismic profiling applied to sedimentology: Geophysics, v. 53, p. 1276-1283.

Kilty, K.T., and A.L. Lange, 1990, Acoustic tomography in shallow geophysical exploration using a transform reconstruction: Soc. Explor. Geophys. Investigations in Geophysics no. 5, S.H. Ward, ed., Vol. 3: Geotechnical, p. 23-35.

Lankston, R.W., 1990, High-resolution refraction seismic data acquisition and interpretation: Soc. Explor. Geophys. Investigations in Geophysics no. 5, Stan H. Ward, ed., Volume 1: Review and Tutorial, p. 45-73.
Lytle, R.J. and K.A. Dines, 1980, Iterative ray tracing between boreholes for underground image reconstruction: Inst. Electr. Electron. Eng. Trans. Geosci. Remote Sensing, v. GE-18, p. 234-240.
Menke, W., 1984, Geophysical data analysis—Discrete inversion theory: Academic Press, Inc., New York.
Michaels, P., 1999, Use of engineering geophysics in the design of highway passing lanes: Proceedings of the Symposium on the Application of Geophysics to Engineering and Environmental Problems (SAGEEP 1999), Oakland, Calif., March 14-18, p. 179-187.
Miller, R.D., and J. Xia, 1999, Using MASW to map bedrock in Olathe, Kansas: Kansas Geological Survey Open-file Report 99-9.
Miller, R.D., D.W. Steeples, and M. Brannan, 1989, Mapping a bedrock surface under dry alluvium with shallow seismic reflections: Geophysics, v. 54, p. 1528-1534.
Miller, R.D., N.L. Anderson, H.R. Feldman, and E.K. Franseen, 1995, Vertical resolution of a seismic survey in stratigraphic sequences less than 100 m deep in Southeastern Kansas: Geophysics, v. 60, p. 423-430.
Millet, J.A., and H.F. Barnett, 1970, Surface materials and terrain features of Yuma Proving Ground: United States Army Natick Laboratories, Technical report 71-14-ES, Earth Sciences Laboratory ES-59.
Mooney, H.M., 1981, Handbook of engineering geophysics: Bison Instruments, Inc.
Nazarian, S., K.H. Stokoe II, and W.R. Hudson, 1983, Use of spectral analysis of surface waves method for determination of moduli and thicknesses of pavement systems: Transportation Research Record No. 930, p. 38-45.
Olea, R.A., 1999, Geostatistics for engineers and earth scientists: Kluwer Academic Publishers, Boston, 303 p.
Palmer, D., 1981, An introduction to the generalized reciprocal method of seismic refraction interpretation: Geophysics, v. 46, p. 1508-1518.
Park, C.B., R.D. Miller, D.W. Steeples, and R.A. Black, 1996, Swept impact seismic technique (SIST): Geophysics, v. 61, p. 1789-1803.
Park, C.B. R.D. Miller, and J. Xia, 1999, Multichannel analysis of surface waves (MASW): Geophysics, v. 64, p. 800-808.
Peterson, J.E., Paulsson, B.N.P., and T.A. McEvilly, 1985, Applications of algebraic reconstruction techniques to cross-hole data: Geophysics, v. 53, p. 1284-1294.
Pullan, S.E., and J.A. Hunter, 1990, Delineation of buried bedrock valleys using the optimum offset shallow seismic reflection technique: Soc. Explor. Geophys. Investigations in Geophysics no. 5, S.H. Ward, ed., Volume 3: Geotechnical, p. 75-87.
Redpath, B.B., 1973, Seismic refraction exploration for engineering site investigations, NTIS AD-768710.
Sander, J.E., 1978, The blind zone in seismic ground-water exploration: Ground Water, v. 165, p. 394-397.
Schneider, W.A., Jr., K.A. Ranzinger, A.H. Balch, and C. Kruse, C., 1992, A dynamic programming approach to first arrival traveltime computation in media with arbitrarily distributed velocities: Geophysics, v. 57, p. 39-50.
Scott, J.H., 1977, SIPT–A seismic refraction inverse modeling program for timeshare terminal computer systems: U.S. Geological Survey Open-file Report 77-365.
Schepers, R., 1975, A seismic reflection method for solving engineering problems: Journal of Geophysics, v. 41, p. 267-284.
Shtivelman, V., U. Frieslander, E. Zilberman, and R. Amit, 1998, Mapping shallow faults at the Evrona playa site using high-resolution reflection method: Geophysics, v. 63, p. 1257-1264.
Soske, J.L., 1954, The blind zone problem in engineering geophysics: Geophysics, v. 24, p. 359-365.
Steeples, D.W., and R.D. Miller, 1990, Seismic reflection methods applied to engineering, environmental, and groundwater problems: Soc. Explor. Geophys. Investigations in Geophysics no. 5, Stan H. Ward, ed., Volume 1: Review and Tutorial, p. 1-30.
Steeples, D.W., C.M. Schmeissner, and B.K. Macy, 1995, The evolution of shallow seismic methods: Journal of Environmental and Engineering Geophysics, v. 0, n. 1, p. 15-24 (invited paper).
Steinhart, J.S., and R.P. Meyer, 1961, Explosion studies of continental structure: Carnegie Institution of Washington Publication 622.
Stokoe II, K.H., G.W. Wright, A.B. James, and M.R. Jose, 1994, Characterization of geotechnical sites by SASW method: in Geophysical Characterization of Sites, ISSMFE Technical Committee #10, ed. R.D. Woods, Oxford Publishers, New Delhi.
Xia, J., Miller, R.D., and Park, C.B., 1999, Estimation of near-surface shear-wave velocity by inversion of Rayleigh wave: *Geophysics*, v. 64, p. 691-700.
Xia, J., R.D. Miller, and C.B. Park, 2000, Advantages of calculating shear-wave velocity from surface waves with higher modes: [Exp. Abs.]: Soc. Expl. Geophys., p. 1295-1298.
Xia, J., R.D. Miller, and C.B. Park, 2001, Feasibility of determining Q of near-surface materials from Rayleigh waves [Exp. Abs.]: Soc. Expl. Geophys., p. 1381-1384.